Supporting Information

Well-Coupled Nanohybrids Obtained by Component-Controlled Synthesis and In-Situ Integration of Mn_xPd_y Nanocrystals on Vulcan Carbon for Electrocatalytic Oxygen Reduction

Yanan Lu,[†] Shulin Zhao,[†,‡] Rui Yang,[†,§] Dongdong Xu,[†] Jing Yang,[†] Yue Lin,[‡,*] Nai-En Shi,[§] Zhihui Dai,[†] Jianchun Bao,[†] and Min Han[†,⊥,*]

[†]Jiangsu Key Laboratory of Biofunctional Materials, School of Chemistry and Materials Science, Nanjing Normal University, Nanjing 210023, P. R. China

[‡] Hefei National Laboratory for Physical Sciences at the Microscale, University of Science & Technology of China, Hefei 230026, China

[§]Key Laboratory for Organic Electronics and Information Displays, Institute of Advanced Materials, Nanjing University of Posts & Telecommunications, Nanjing 210023, P. R. China

[⊥]State Key Laboratory of Coordination Chemistry, Nanjing National Laboratory of Solid State Microstructures, Nanjing University, Nanjing 210093, P. R. China

* To whom correspondence should be addressed.

E-mail: linyue@ustc.edu.cn (Dr. Y. Lin); 07203@njnu.edu.cn (Prof. Dr. M. Han)

Phone/Fax: +86-25-85891051.

This information contains:

(1) Characterization of Vulcan XC-72 C before and after acidic treatment (**Figure S1**)

(2) EDS pattern, magnified Raman and survey XPS spectra for $MnPd_3$/C NHs (**Figure S2-4**)

(3) Characterization of Pd/C catalyst (**Figure S5**)

(4) N_2 adsorption-desorption test plots for $MnPd_3$/C NHs (**Figure S6**)

(5) Characterization of other Mn_xPd_y/C NHs control catalysts (**Figure S7-9**)

(6) Additional electrochemical data for $MnPd_3$/C NHs and Pt/C catalyst (**Figure S10-11, Table S1,** and **Figure S12-13**)

(7) Characterization of pure $MnPd_3$ NCs (**Figure S14**)

(8) Comparing the ORR polarization plots of $MnPd_3$/C NHs with that of pure Vulcan XC-72 C, pure $MnPd_3$ NCs, and Pt/C catalyst (**Figure S15**)

(9) Comparing the XPS and electrochemical impedance spectra of $MnPd_3$/C NHs and pure $MnPd_3$ NCs (**Figure S16**)

Additional Experimental Sections

Pre-treatment of Vulcan XC-72 carbon. In a typical synthesis, 2.0 g of Vulcan XC-72 carbon, 30 mL of deionized water and 15 mL of HNO_3 were added into a clean three-necked flask in turn. Subsequently, the reactor was heated from room temperature to 90 ^oC under violently magnetic stirring and kept at 90 ^oC for 5 h. After naturally cooled down to room temperature, the crude product was separated by centrifugation, which was further washed with deionized water and diluted ammonium hydroxide solution for several times until the supernatant solution became neutral. Finally, the black product was dried in vacuum at 40 ^oC for overnight, and used for the subsequent synthesis and characterization.

Koutecky-Levich (K-L) plots. To get some insight on the catalytic behaviours, the ORR on $MnPd_3$/C NHs was further investigated by rotating disk voltammetry (RDV). The related ORR polarization curves at the rotating rate of 400, 800, 1200, 1600, and 2500 rpm were obtained. Based on those polarization curves, the number of transferred electrons (*n*) involved in the ORR process can be calculated according to following Koutecky-Levich (K-L) equation:

$$\frac{1}{J} = \frac{1}{J_K} + \frac{1}{B\omega^{0.5}} \qquad (1)$$

$$\mathrm{B} = 0.62\mathrm{nF}(D_{O_2})^{2/3}\mathrm{v}^{-1/6}C_{O_2} \qquad (2)$$

Where J is the current density, J_k is the kinetic current density, ω is the rotating rate of the electrode, and B could be obtained from the K-L plots using the equation (1). In addition, F in the equation (2) is the Faraday constant (96485 C mol^{-1}), D_{O2} is the diffusion coefficient of O_2 in 0.1 M KOH (1.9×10^{-5} cm^2 s^{-1}), v is the kinetic viscosity (0.01 cm^2 s^{-1}), C_{O2} is the bulk

concentration of O_2 (1.2×10^{-6} mol cm^{-3}), and the value of *n* represents the number of transferred electrons in the ORR process.

Rotating ring-disk electrode (RRDE) measurements. The rotating speed of the working electrode was fixed at 1600 rpm with the scan rate of 5 mV s^{-1} in O_2-saturated 0.1 M KOH solution for the RRDE test. The number of transferred electrons (*n*) and the yield of HO_2^- species involved in the ORR process were calculated according to the following equations:

$$n = 4I_d/(I_d + I_r/N) \quad (3)$$

$$HO_2^-\% = 200(I_r/N)/(I_d + I_r/N) \quad (4)$$

Where I_d stands for the disk current, I_r represents the ring current, and N is the current collection efficiency of the Pt ring, which is identified to be 0.43 in 2 mmol L^{-1} $K_3[Fe(CN)_6]$ and 0.1 mol L^{-1} KCl solution.

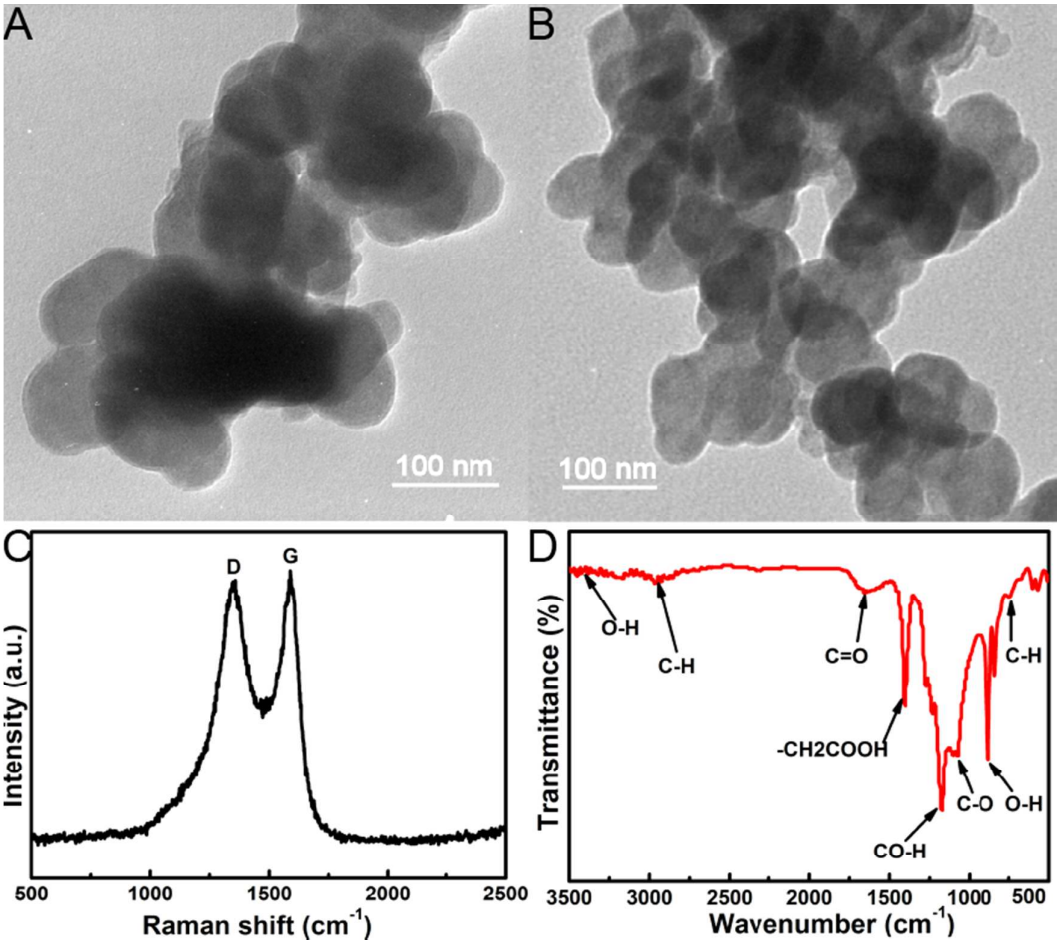

Figure S1. A-B) TEM images of the Vulcan XC-72 C before and after acidic treatment. C-D) Raman (C) and FT-IR (D) spectra of the Vulcan XC-72 C after acidic treatment.

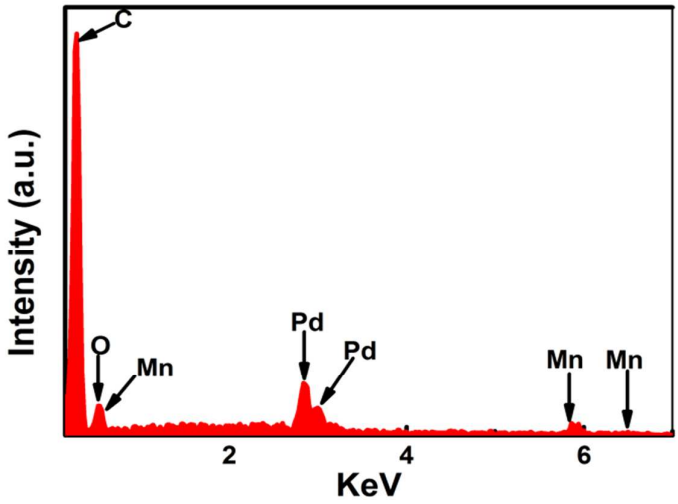

Figure S2. The EDS pattern for the typical $MnPd_3$/C NHs.

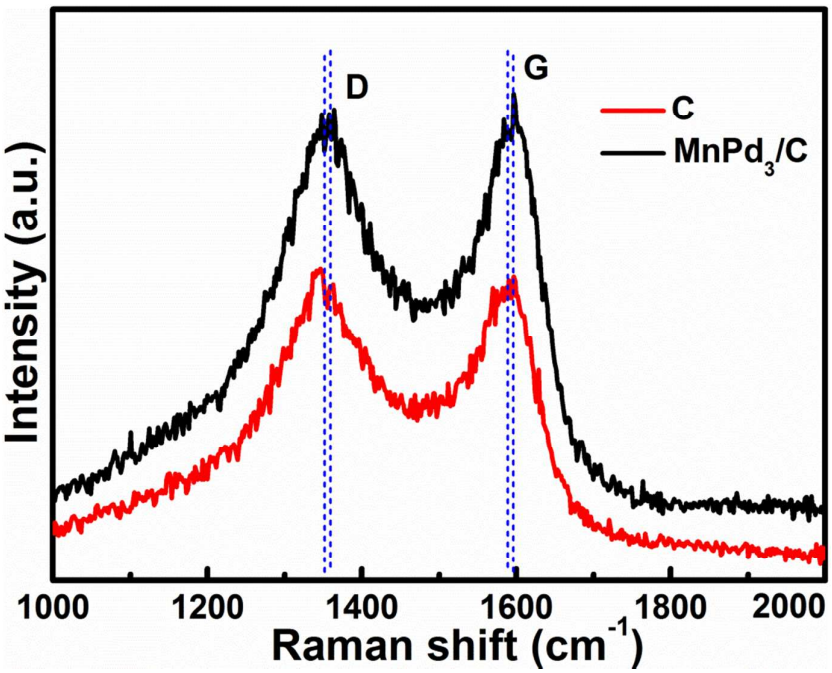

Figure S3. The magnified Raman spectra for the $MnPd_3$/C NHs and Vulcan XC-72 C at the wavenumber ranging from 1000 to 2000 cm^{-1}.

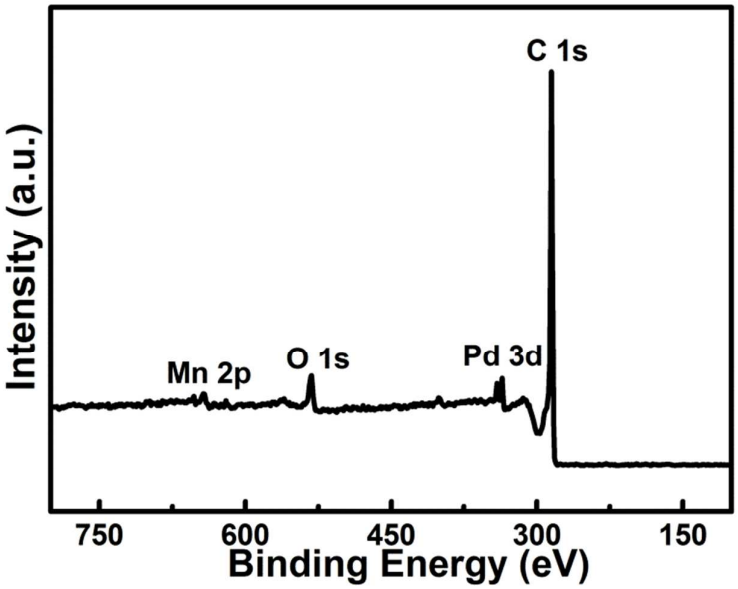

Figure S4. The survey XPS spectrum for the typical $MnPd_3$/C NHs.

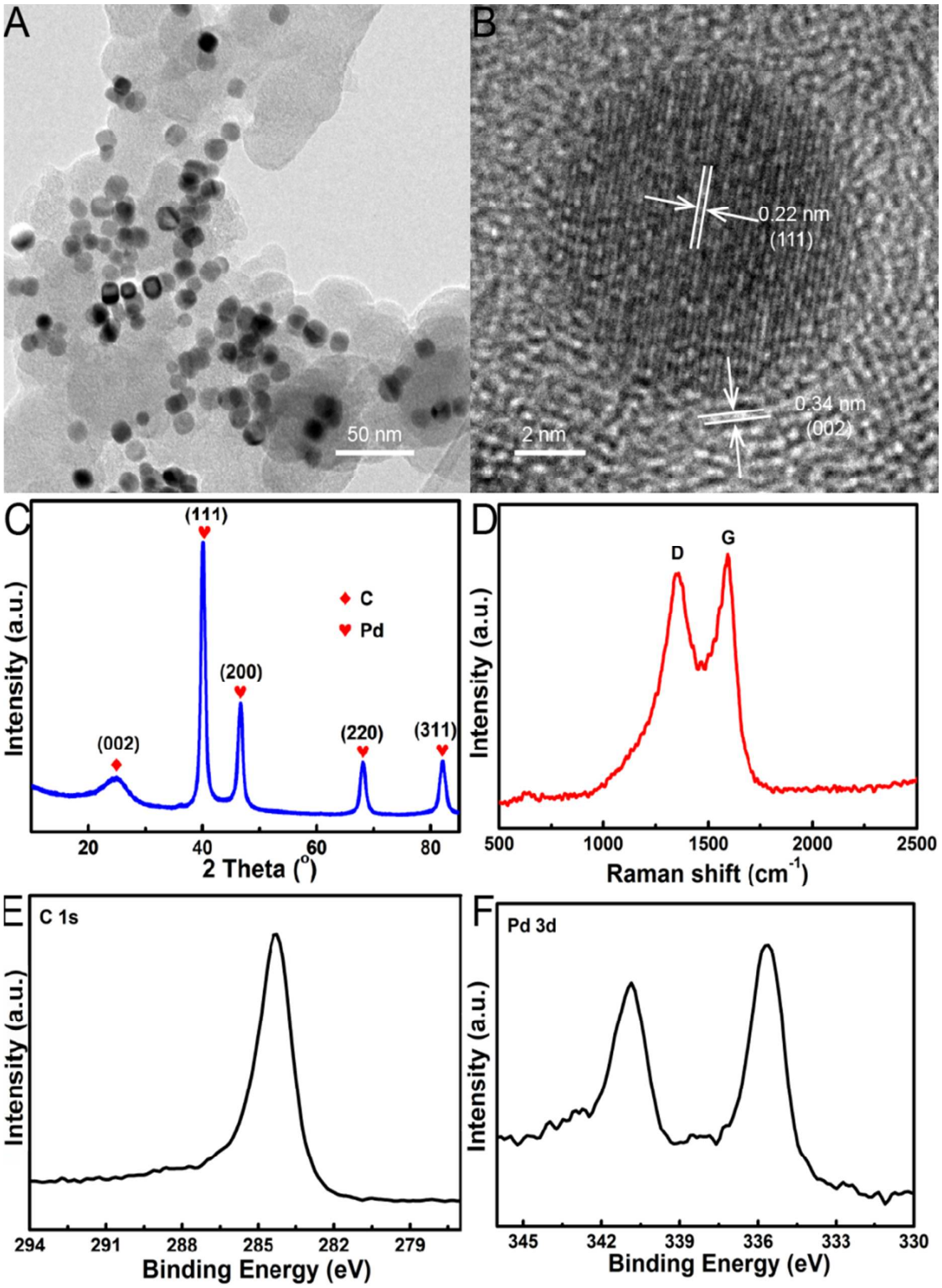

Figure S5. A-B) The representative TEM (A) and HRTEM (B) images for the Pd/C NHs

control catalyst. C-D) Related powder XRD pattern (C) and Raman spectrum (D) of the Pd/C NHs control catalyst. E-F) The core-level XPS spectra for the C 1s (E) and Pd 3d (F) peaks, respectively.

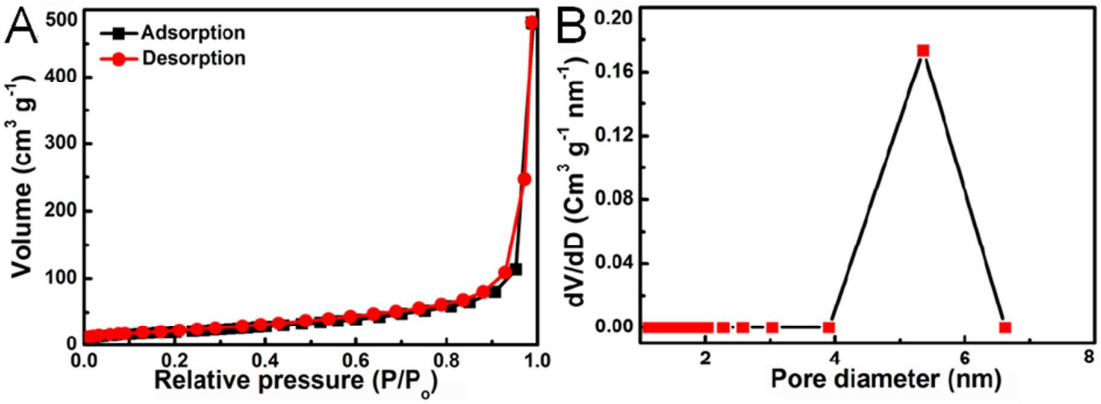

Figure S6. N_2 adsorption-desorption tests for $MnPd_3$/C NHs. A) The adsorption-desorption isothermal plots. B) The corresponding pore size distribution curve.

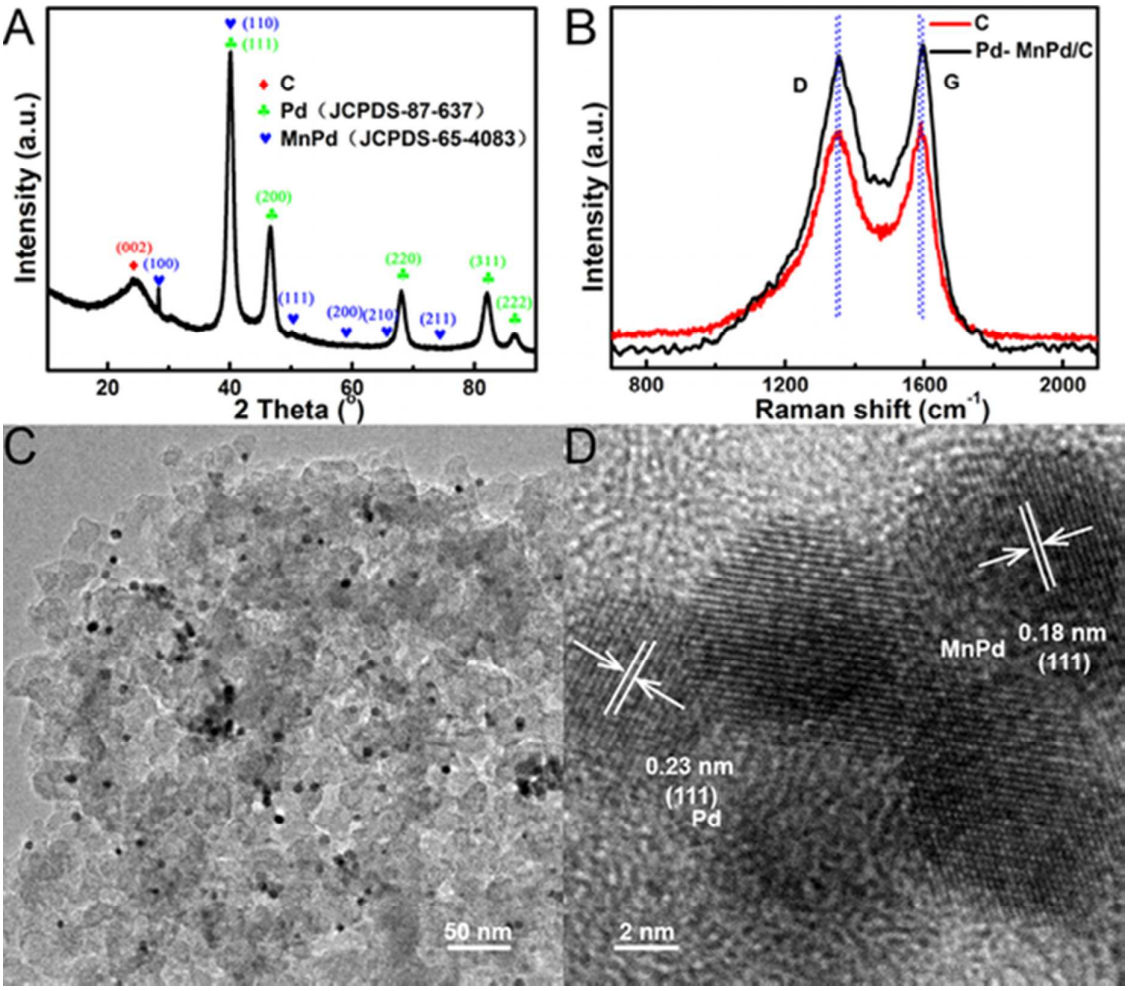

Figure S7. A) The XRD pattern of the MnPd-Pd/C NHs that obtained by changing the molar ratio of the initial Mn and Pd precursors to be 1:5 and keeping other conditions constant. B) Comparison of the Raman spectrum of MnPd-Pd/C NHs with that of pure Vulcan XC-72 C. C-D) The corresponding TEM (C) and HRTEM (D) images for the obtained MnPd-Pd/C NHs.

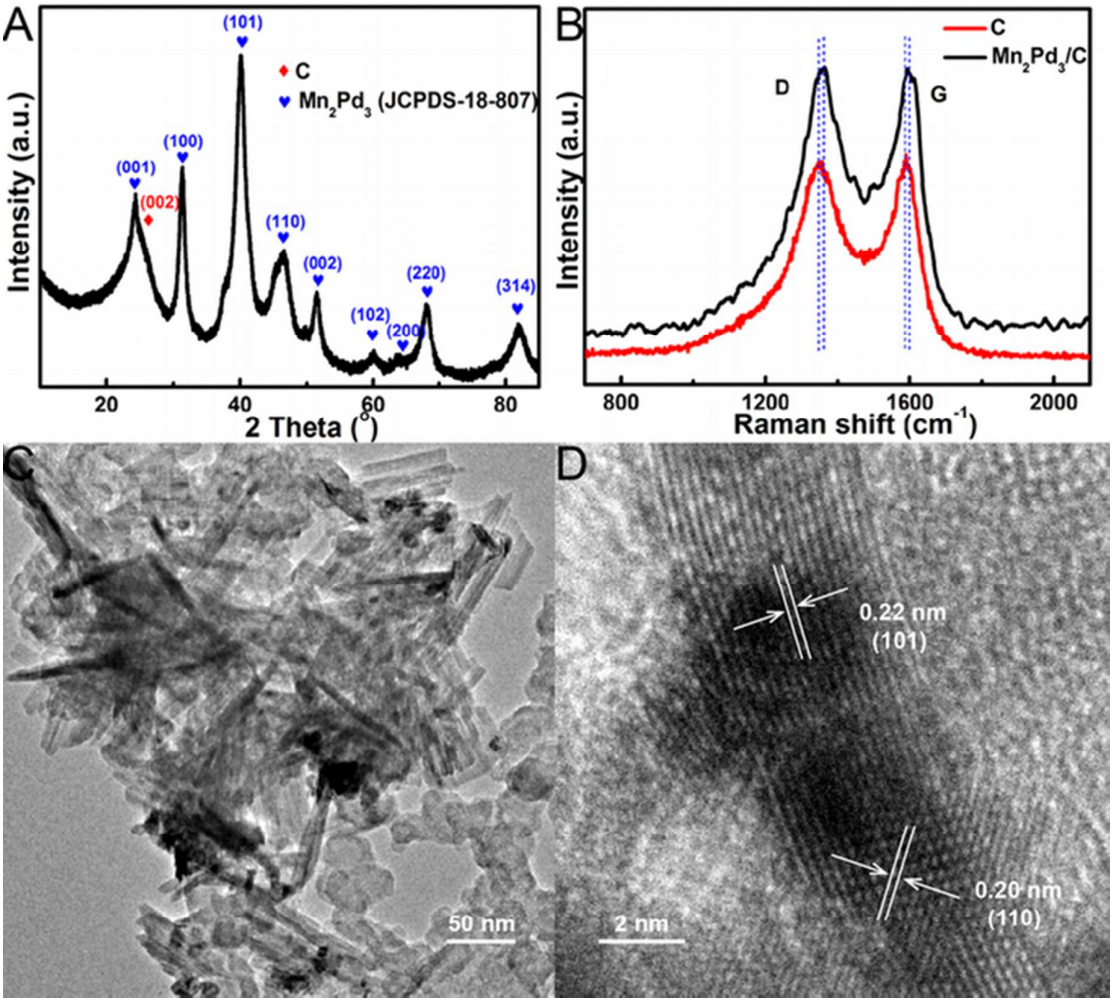

Figure S8. A) The XRD pattern of the Mn_2Pd_3/C NHs that obtained by changing the molar ratio of the initial Mn and Pd precursors to be 1:1 and keeping other conditions constant. B) Comparison of the Raman spectrum of Mn_2Pd_3/C NHs with that of pure Vulcan XC-72 C. C-D) The corresponding TEM (C) and HRTEM (D) images for the obtained Mn_2Pd_3/C NHs.

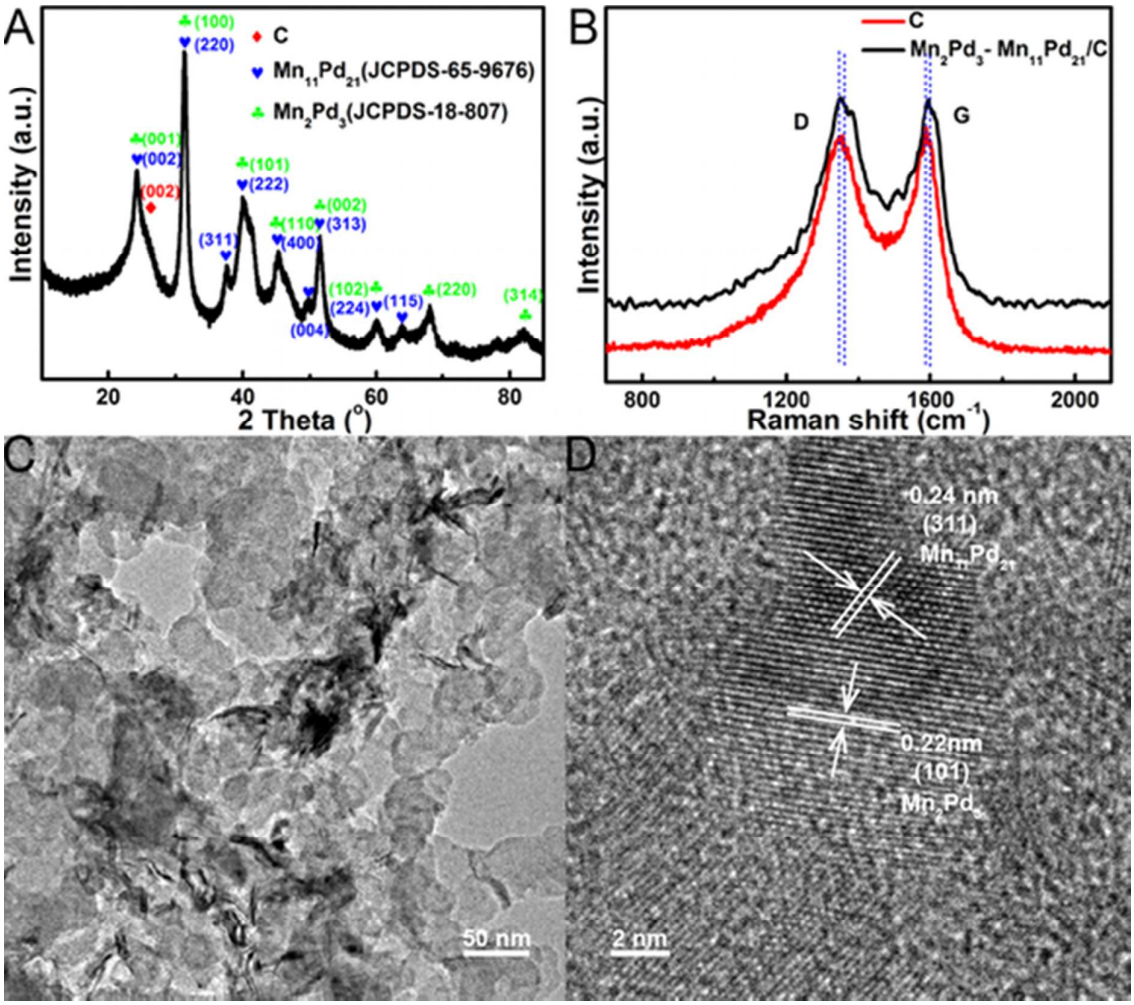

Figure S9. A) The XRD pattern of the Mn_2Pd_3-$Mn_{11}Pd_{21}$/C NHs that obtained by changing the molar ratio of the initial Mn and Pd precursors to be 3:1 and keeping other conditions unchanged. B) Comparison of the Raman spectrum of the Mn_2Pd_3-$Mn_{11}Pd_{21}$/C NHs with that of pure Vulcan XC-72 C. C-D) The corresponding TEM (C) and HRTEM (D) images for the obtained Mn_2Pd_3-$Mn_{11}Pd_{21}$/C NHs.

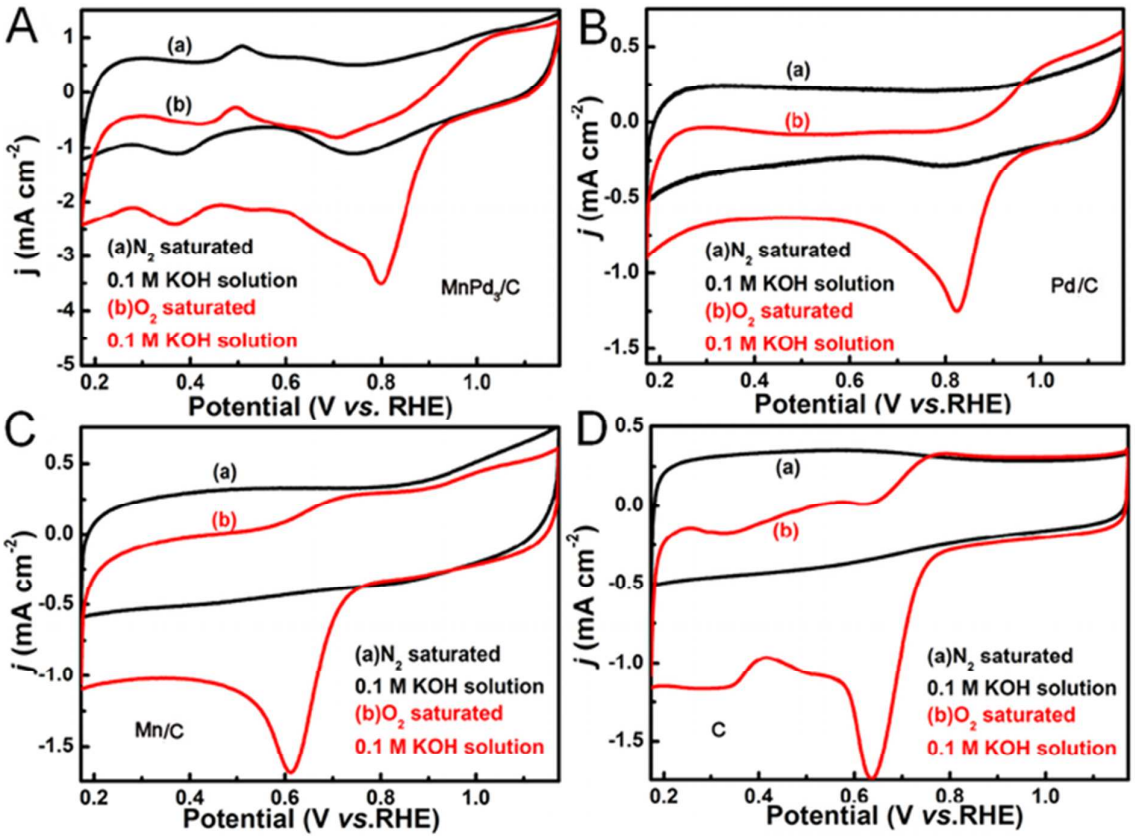

Figure S10. A) CV curves for the $MnPd_3$/C NHs in N_2- and O_2-saturated 0.1 M KOH electrolyte at the potential window of 0.17 to 1.17 V (*vs*. RHE) and the scan rate of 100 mV s^{-1}. B-D) Corresponding CV plots for pure Pd/C NHs (B), Mn/C NHs (C), and Vulcan XC-72 C (D) in N_2- and O_2-saturated 0.1 M KOH electrolyte under the same potential window and scan rate.

[**Assignments**] By comparison of the CV curves of $MnPd_3$/C NHs (**Figure S10A**) with that of pure Pd/C (**Figure S10B**), Mn/C (**Figure S10C**) NHs and Vulcan XC-72 C (**Figure S10D**), the first pair of redox peaks for $MnPd_3$/C NHs at the potential of 0.17 to 0.3 V (*vs*. RHE) is assigned to H_{upd} adsorption-desorptuon peaks, respectively. The second pair of redox peaks at the potential of 0.3 to 0.5 V (*vs*. RHE) and the third pair of small redox peaks at the potential ranging from 0.5 to 0.7 V (*vs*. RHE) are attributed to the Mn redox peaks, respectively. As for the fourth pair of redox peaks at 0.7 to 1.1 V (*vs*. RHE) may be attributed to the Pd redox peaks, respectively.

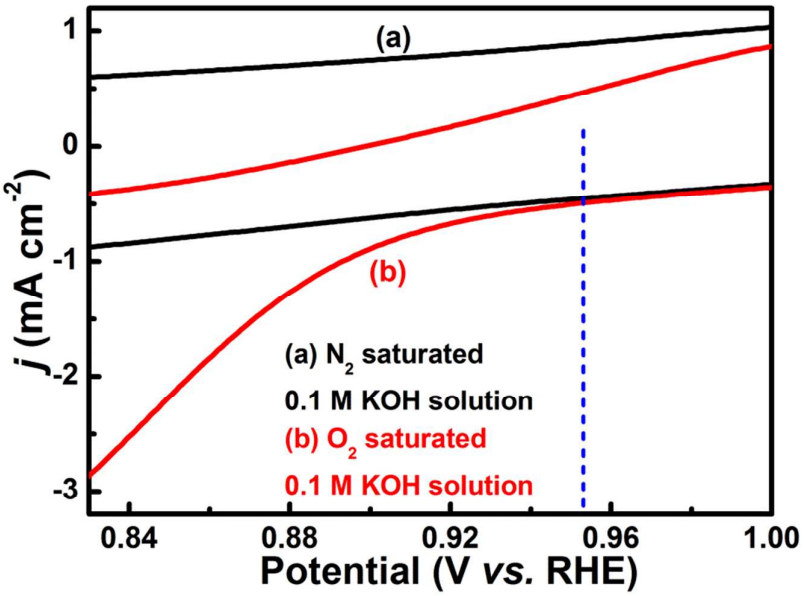

Figure S11. The magnified CVs of the $MnPd_3$/C NHs in N_2- and O_2-saturated 0.1 M KOH electrolyte at the potential window of 0.83 to 1.0 V (*vs*. RHE).

Table S1. Comparing the catalytic performance parameters of our $MnPd_3$/C NHs with recently reported some non-Pt electrocatalysts

Catalysts	Electrolyte	E_o V (*vs*. RHE)	$E_{1/2}$ V (*vs*. RHE)	Tafel Slope (mV dec^{-1})	References
Ag-Co	0.1 M NaOH	~0.95	-	-	(1)
AuCu	1.0 M KOH	0.925	-	-	(2)
Pd_2NiAg	0.1 M KOH	0.923	0.842	-	(3)
PdCuCo	0.1 M KOH	-	0.872	-	(4)
PdCuNi		-	0.862	-	
Pd-HPW-CMK	0.1 M KOH	0.901	-	76.9	(5)
Pd-g-C_3N_4	0.1 M KOH	0.90	-	-	(6)
Co−N/CNFs	0.1 M KOH	0.92	0.82	-	(7)

Co-N-CNT	0.1 M KOH	0.93	0.82	-	(8)
G-Cu_3Pd	0.1 M KOH	0.952	-	68.9	(9)
G-$FePd_3$	0.1 M KOH	0.925	-	-	(10)
Pd_3Pb/C	0.1 M KOH	~1.03	0.92	-	(11)
Pd_3Fe/C	0.1 M KOH	~1.05	-	71.4	(12)
PdCo/NPC	0.1 M KOH	0.928	0.843	-	(13)
AuPdCo/C	0.1 M KOH	~1.0	-	-	(14)
PdNiCu/NG PdNiSn/NG	0.1 M KOH	-	0.763	-	(15)
NS-3DrGO-950	0.1 M KOH	0.895	0.732	92	(16)
$MnPd_3$/C	**0.1 M KOH**	**0.953**	**0.8**	**65**	**This work**

[notes] The symbols of "E_o" and "$E_{1/2}$" represent the "**onset reduction potential**" and "**half-wave potential**", respectively. And the symbol of "-" means that the related parameter has not been mentioned in the literature. The abbreviations of "G" and "N-G" stand for the "**graphene**" and "**N-doped graphene**", respectively. And the abbreviation of "NPC" represents the "**N-doped porous carbon**". The abbreviations of "CNF" and "CNT" stand for the "**carbon nanofibers**" and "**carbon nanotubes**", respectively. The abbreviation of "NS" stands for "**N,S-codoped**". And the symbol of "rGO" means the "**reduced graphene oxides**".

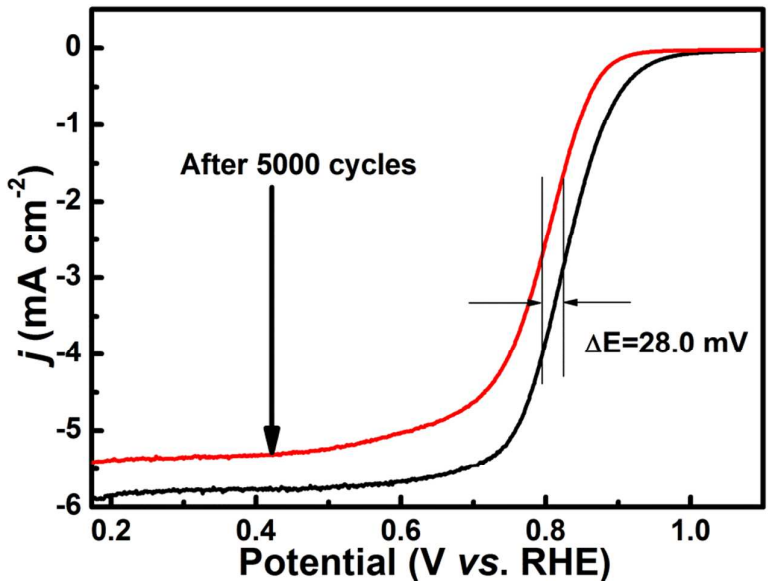

Figure S12. The durability test plots for commercial Pt/C catalyst.

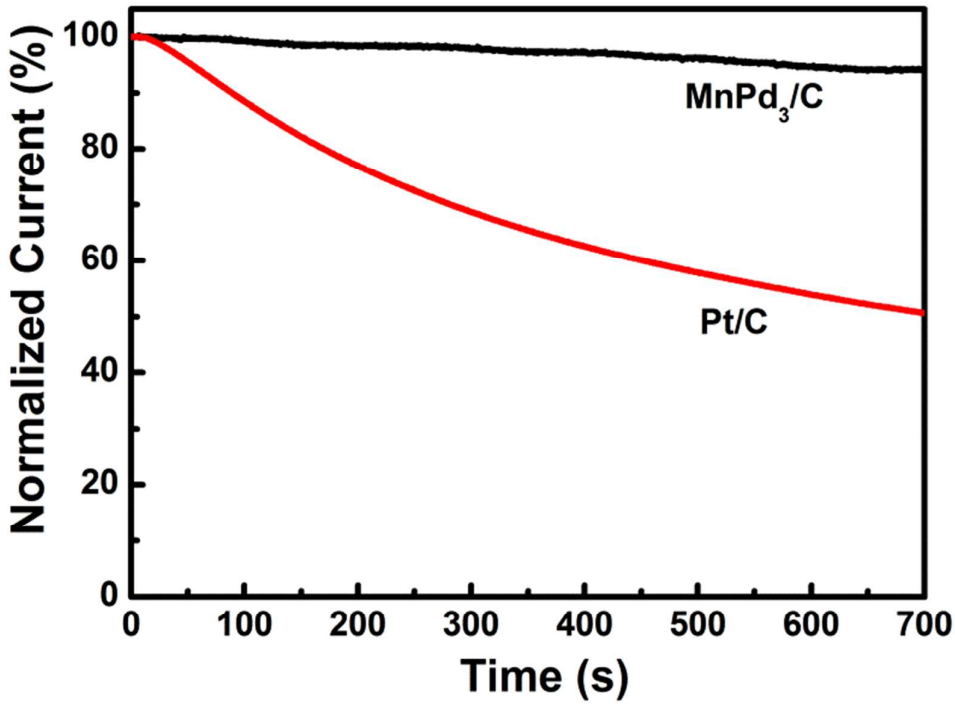

Figure S13. Chronoamperometric responses of the typical $MnPd_3$/C NHs and Pt/C catalyst at a constant potential of 0.7 V (*vs*. RHE) in O_2-saturated 0.1 M KOH + 1 M CH_3OH solution with the electrode rotation rate of 1600 rpm.

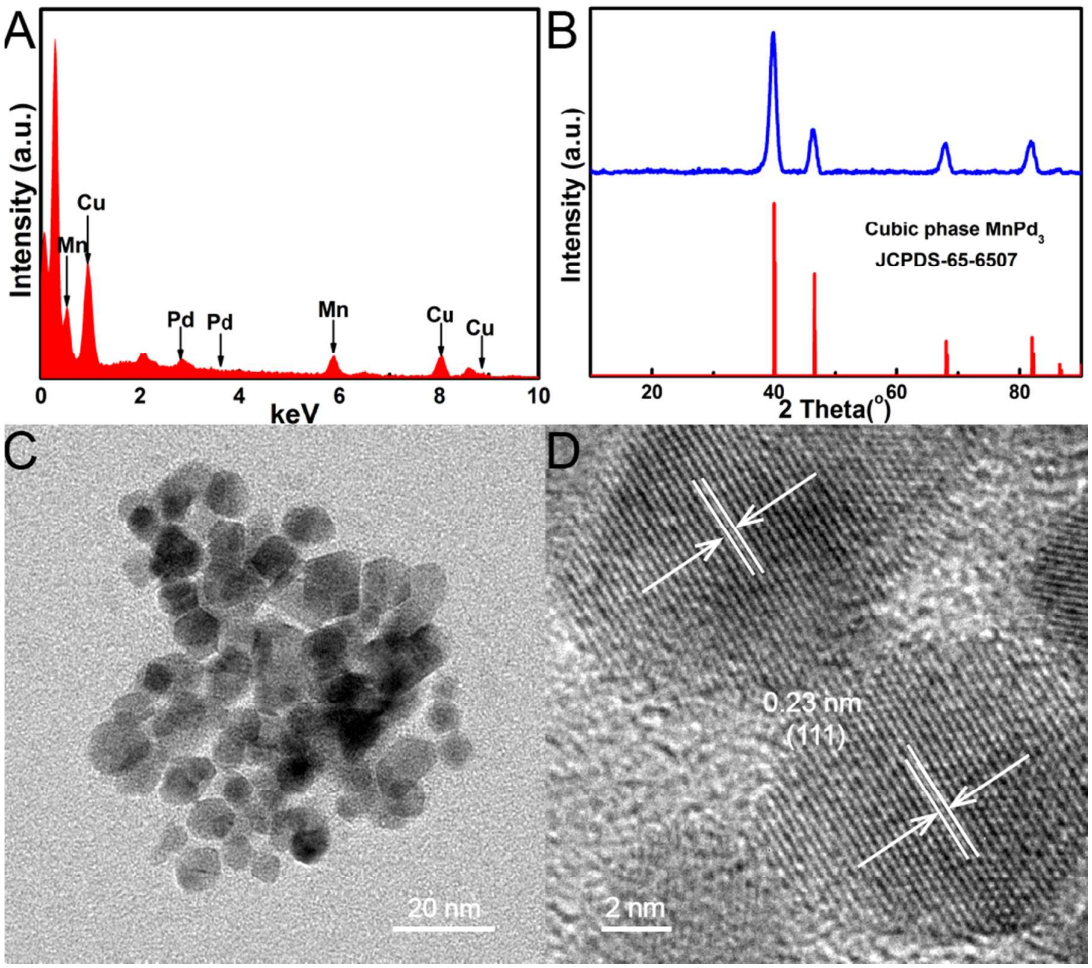

Figure S14. A-B) The EDS spectrum (A) and powder XRD pattern (B) of pure $MnPd_3$ nanocrystals. C-D) Corresponding TEM (C) and HRTEM (D) images for pure $MnPd_3$ nanocrystals. It should be mentioned that the EDS pattern of this sample is taken from the TEM apparatus. The signal of Cu element originates from the used copper grid.

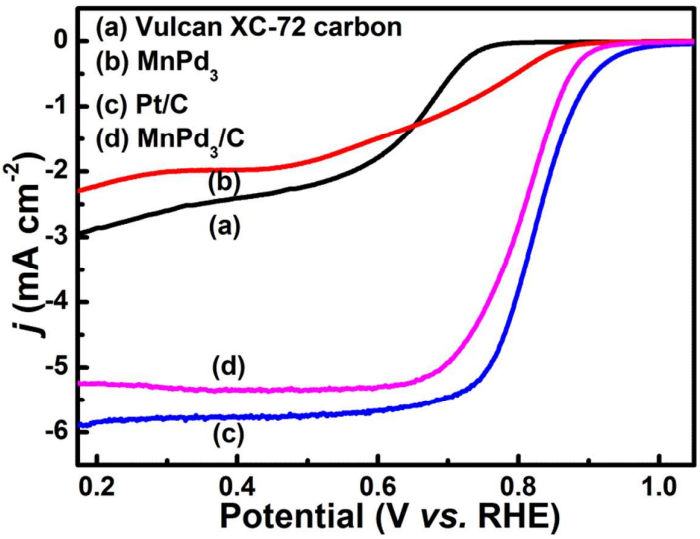

Figure S15. ORR polarization plots of pure Vulcan XC-72 C (a), pure $MnPd_3$ nanocrystals (b), commercial Pt/C (c), and the $MnPd_3$/C NHs (d) in O_2-saturated 0.1 M KOH electrolyte at the electrode rotation rate of 1600 rpm.

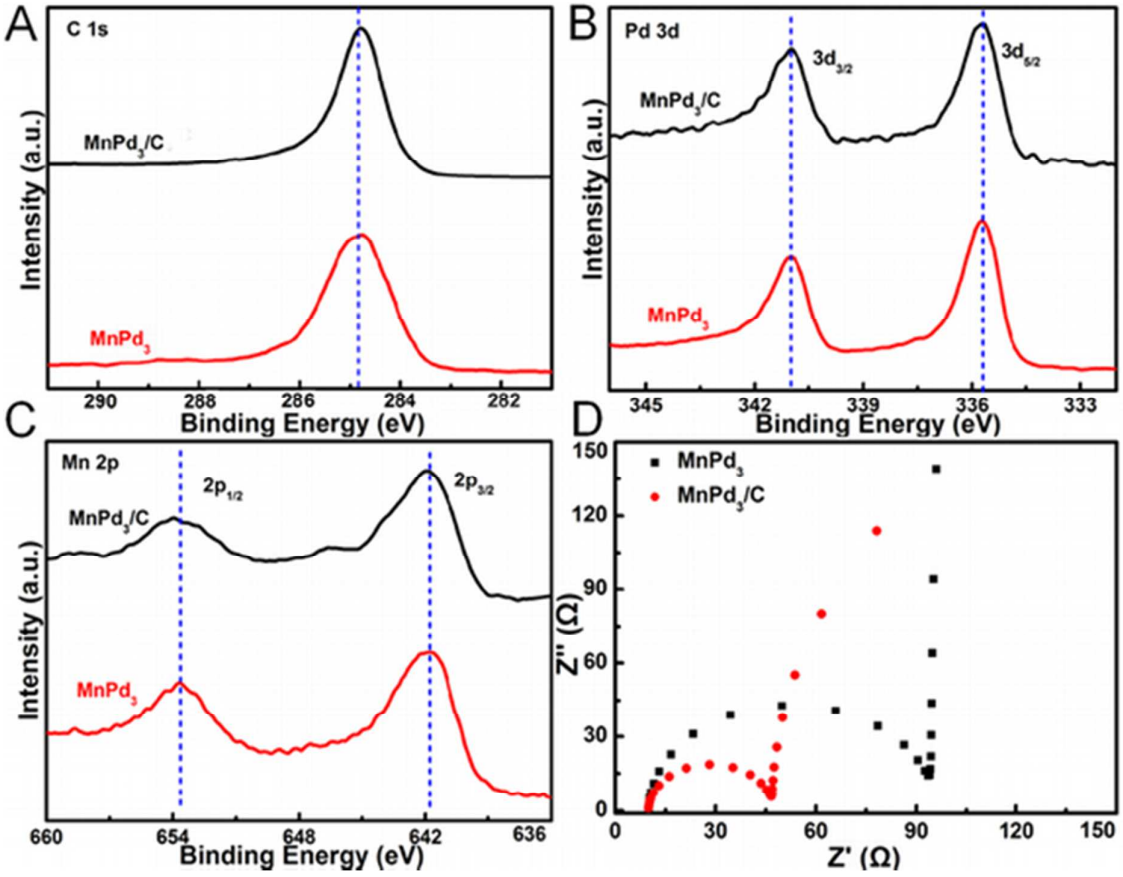

Figure S16. A-C) Comparison of the C 1s (A), Pd 3d (B), and Mn 2p (C) core-level XPS spectra for $MnPd_3$/C NHs and pure $MnPd_3$ NCs, repectively. D) The Nyquist plots for $MnPd_3$/C NHs (red plot) and pure $MnPd_3$ NCs (black plot).

References

(1) Holewinski, A.; Idrobo, J. C.; Linic, S. High-performance Ag-Co Alloy Catalysts for Electrochemical Oxygen Reduction. *Nat. Chem*. **2014**, *6*, 828-834.

(2) Wang, G.; Xiao, L.; Huang, B.; Ren, Z.; Tang, X.; Zhuang, L.; Lu, J. AuCu Intermetallic Nanoparticles: Surfactant-Free Synthesis and Novel Electrochemistry. *J. Mater. Chem.* **2012**, *22*, 15769-15774.

(3) Liu, S.; Zhang, Q.; Li, Y.; Han, M.; Gu, L.; Nan, C.; Bao, J.; Dai, Z. Five-Fold Twinned Pd_2NiAg Nanocrystals with Increased Surface Ni Site Availability to Improve Oxygen Reduction Activity. *J. Am. Chem. Soc.* **2015**, *137*, 2820-2823.

(4) Jiang, K.; Wang, P.; Guo, S.; Zhang, X.; Shen, X.; Lu, G.; Su, D.; Huang, X. Ordered PdCu-Based Nanoparticles as Bifunctional Oxygen-Reduction and Ethanol-Oxidation Electrocatalysts. *Angew. Chem., Int. Ed*. **2016**, *55*, 1-7.

(5) Liu, H.; Zheng, Y.; Wang, G.; Qiao, S. Z. A Three-Component Nanocomposite with Synergistic Reactivity for Oxygen Reduction Reaction in Alkaline Solution. *Adv. Energy Mater*. **2015**, *5*, 1401186.

(6) Konda, S. K.; Amiri, M.; Chen, A. Photoassisted Deposition of Palladium Nanoparticles on Carbon Nitride for Efficient Oxygen Reduction. *J. Phys. Chem. C* **2016**, *120*, 14467 -14473.

(7) Cheng, Q.; Yang, L.; Zou, L.; Zou, Z.; Chen, C.; Hu, Z.; Yang, H. Single Cobalt Atom and N Codoped Carbon Nanofibers as Highly Durable Electrocatalyst for Oxygen Reduction Reaction. *ACS Catal*. **2017**, *7*, 6864-6871.

(8) Kim, S.; Jang, D.; Lim, J.; Oh, J.; Kim, S. O.; Park, S. Cobalt-Based Active Species Molecularly Immobilized on Carbon Nanotubes for the Oxygen Reduction Reaction. *ChemSusChem* **2017**, *10*, 3473-3481.

(9) Zheng, Y.; Zhao, S.; Liu, S.; Yin, H.; Chen, Y. Y.; Bao, J.; Han, M.; Dai, Z. Component-Controlled Synthesis and Assembly of Cu-Pd Nanocrystals on Graphene for Oxygen Reduction Reaction. *ACS Appl. Mater. Interfaces* **2015**, *7*, 5347-5357.

(10) Yin, H.; Liu, S.; Zhang, C.; Bao, J.; Zheng, Y.; Han, M.; Dai, Z. Well-Coupled Graphene

and Pd-Based Bimetallic Nanocrystals Nanocomposites for Electrocatalytic Oxygen Reduction Reaction. *ACS Appl. Mater. Interfaces* **2014**, *6*, 2086-2094.

(11) Cui, Z.; Chen, H.; Zhao, M.; DiSalvo, F. J. High-Performance Pd_3Pb Intermetallic Catalyst for Electrochemical Oxygen Reduction. *Nano Lett*. **2016**, *16*, 2560-2566.

(12) Cui, Z.; Li, L.; Manthiram, A.; Goodenough, J. B. Enhanced Cycling Stability of Hybrid Li-Air Batteries Enabled by Ordered Pd_3Fe Intermetallic Electrocatalyst. *J. Am. Chem. Soc.* **2015**, *137*, 7278-7281.

(13) Xue, H.; Tang, J.; Gong, H.; Guo, H.; Fan, X.; Wang, T.; He, J.; Yamauchi, Y. Fabrication of PdCo Bimetallic Nanoparticles Anchored on Three-Dimensional Ordered N-Doped Porous Carbon as an Efficient Catalyst for Oxygen Reduction Reaction. *ACS Appl. Mater. Interfaces* **2016**, *8*, 20766-20771.

(14) Kuttiyiel, K. A.; Sasaki, K.; Su, D.; Wu, L.; Zhu, Y.; Adzic, R. R. Gold-Promoted Structurally Ordered Intermetallic Palladium Cobalt Nanoparticles for the Oxygen Reduction Reaction. *Nat. Commun*. **2014**, *5*, 5185.

(15) Sun, L.; Liao, B.; Ren, X.; Li, Y.; Zhang, P.; Deng, L.; Gao, Y. Ternary PdNi-based Nanocrystals Supported on Nitrogen-Doped Reduced Graphene Oxide as Highly Active Electrocatalysts for the Oxygen Reduction Reaction. *Electrochim. Acta* **2017**, *159*, 543-552.

(16) Li, Y.; Yang, J.; Huang, J.; Zhou, Y.; Xu, K.; Zhao, N.; Cheng, X. Soft Template-Assisted Method for Synthesis of Nitrogen and Sulfur Co-doped Three-Dimensional Reduced Graphene Oxide as an Efficient Metal Free Catalyst for Oxygen Reduction Reaction. *Carbon* **2017**, *122*, 237-246.